Nucleon-nucleon potentials with and without Δ(1232) degrees of freedom

R. B. Wiringa
Physics Division, Argonne National Laboratory, Argonne, Illinois 60439

R. A. Smith
Department of Physics, Texas A&M University, College Station, Texas 77843

T. L. Ainsworth*
Department of Physics, State University of New York, Stony Brook, New York 11794
(Received 15 April 1983)

We present two new nucleon-nucleon (NN) potentials: a v_{14} model that is a conventional NN potential and a v_{28} model with explicit Δ(1232) degrees of freedom. The v_{14} model has 14 operator components describing NN channels, while the v_{28} model has 14 additional operators, including 12 transition operators for all possible πNΔ and πΔΔ couplings and two central operators for NΔ and ΔΔ channels; the latter are constrained so that the v_{28} model has no additional free parameters for data fitting. The two models give excellent and almost identical fits to deuteron properties and np scattering below 330 MeV. The v_{14} and v_{28} forms are convenient for nuclear structure calculations; when many-body cluster contributions are evaluated the v_{28} model will automatically include much of the effect attributed to many-body forces in conventional models, while the v_{14} model will provide a standard of comparison.

I. INTRODUCTION

Conventional models of the nucleon-nucleon (NN) interaction are built on nonrelativistic protons and neutrons interacting via two-body potentials. Typical NN potentials contain strong short-range repulsion, intermediate-range attraction, and long-range one-pion-exchange (OPE) parts. Nuclear systems are then described by the solution of a many-body Schrödinger equation. We know that such an approach is a great simplification over reality. Nucleons are composite systems with a rich resonance structure, which we now attribute to constituent quarks interacting by gluon exchange. Ideally a model of the NN interaction would start with a field theoretic description of quark-quark interactions, but no satisfactory theory has yet been developed.[1–3] Presumably the quark degrees of freedom only become important at short distances and high energies, so a potential description may be adequate for the realm of low-energy nuclear physics.

The short-range part of the NN potential is generally treated phenomenologically, which is reasonable until a better understanding of the role of quarks is reached. The intermediate-range attraction was at first also described phenomenologically, e.g., as a sum of Yukawa functions in the Reid[4] potential, or as the exchange of a fictitious scalar σ meson, as in the one-boson-exchange (OBE) potentials of the Bonn[5] group. In fact, most of the attraction comes from two-pion-exchange (TPE) processes, such as those shown in Fig. 1, where nucleon resonances may be excited in intermediate states. This feature has been simulated in the Urbana[6] potential, and incorporated by means of the dispersion theory in the Stony Brook[7] and Paris[8] potentials. The Paris potential has long-range and intermediate-range parts completely determined from πN and ππ interactions; for practical many-body calculations it is frequently used in its parametrized form.

The Reid, Bonn, Urbana, Stony Brook, and parametrized Paris potentials may be called "realistic" potentials because they give good fits to deuteron properties and NN scattering data for $E_{\rm lab} \leq 350$ MeV. It was long hoped that such realistic potentials would be adequate for describing nuclear structure and low-energy reactions.[9] However, as our calculational techniques for solving the many-particle Schrödinger equation have improved, this hope has faded. The best perturbative and variational calculations show that with realistic NN potentials the light nuclei ^{3}H and ^{4}He are underbound with too large a charge radius,[10–13] while infinite nuclear matter tends to be overbound, with far too large a saturation density.[14,15] One possible explanation of these results is that the three-

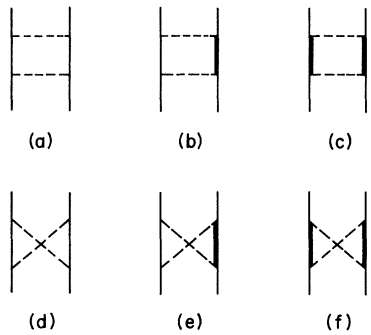

FIG. 1. Two-pion-exchange processes contributing to two-nucleon interaction; solid, heavy, and dashed lines represent N, Δ, and π, respectively.

nucleon interaction is not small and must be considered as an important part of the nuclear Hamiltonian.

The prime example of three-nucleon interaction is the TPE process first described by Fujita and Miyazawa,[16] and illustrated in Fig. 2. The TPE three-nucleon interaction can be written as a three-nucleon potential and its effect on the light nuclei and nuclear matter has been studied by many groups, most recently by Carlson *et al.*[17] There it is found that a TPE three-nucleon potential adjusted in strength to give the correct ^{3}H binding energy will overbind ^{4}He and increase the discrepancy in nuclear matter. However, there should be additional three-body interactions coming from processes, such as those shown in Fig. 3, which are repulsive. Phenomenological potentials including both TPE and repulsive three-body processes give reasonably satisfactory results in light nuclei and nuclear matter. Some problems remain, however, and it would be nice to put the phenomenological repulsive terms on a firmer theoretical footing.

An alternative to the use of phenomenological three-nucleon potentials is to add an additional degree of freedom to the two-body potential, the $\Delta(1232)$ isobar. The $\Delta(1232)$ plays an important role in both the TPE processes which generate the intermediate-range attraction of NN interaction, and in the TPE and repulsive three-nucleon interaction. The $\Delta(1232)$ components can be generated by a generalized OPE potential containing transition operators with $\pi N\Delta$ couplings, as first discussed by Sugawara and von Hippel.[18] Iteration of the generalized OPE potentials in a coupled-channel scheme will simulate the contribution of box diagrams in NN scattering [Figs. 1(a)—(c)] and in three-body clusters will give some, perhaps the dominant part, of TPE three-nucleon attraction [Figs. 2(a) and (b)]. Repulsive three-body contributions will also be generated when diagonal $N\Delta$ interactions are added (Fig. 3). Many additional contributions to NN scattering and three-body forces plus four-body forces, etc., can be generated with such an approach, as illustrated in Fig. 4. Thus a coupled-channel model of NN scattering with $\Delta(1232)$ degrees of freedom may offer some distinct advantages in studies of nuclear many-body systems.

The coupled-channels scheme has limitations. It cannot reproduce the structure of cross-box diagrams [Figs. 1(d)—(f)] for instance. Smith and Pandharipande[19] found cancellations between the cross-box diagrams with the result that a twice-iterated OPE potential with $\pi N\Delta$ couplings could reasonably reproduce the sum of box and cross-box diagrams. They concluded that the coupled-channels scheme was thus a reasonable approach. Durso *et al.*[20] noted that the box and cross-box diagrams are comparable, however, and represent different contributions to the wave function. They emphasized the advantages of a dispersion-theoretic approach which can make contact with knowledge of $\pi\pi$ and πN interactions. The cancellations among cross-box diagrams were also found by Bagnoud *et al.*[21] Portions of the TPE three-nucleon interaction will also be missed, such as the S-wave scattering from Fig. 2(c), which the Tucson[22] group has found to be non-negligible. We take the attitude that transition potentials have considerable merit for use in a many-body Hamiltonian and that it should be possible to compensate for some of the limitations phenomenologically, e.g., by allowing for intermediate-range parts of the NN potential other than just iterated OPE, which could simulate the residual effects of the cross-box diagrams.

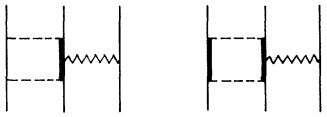

FIG. 3. Repulsive three-nucleon interactions due to $N\Delta$ interaction; wavy line represents π, ρ, or ω exchange.

A considerable amount of work has already been done in the coupled-channel approach, both in constructing potential models and in studying the effect of the added $\Delta(1232)$ degree of freedom in nuclear systems. Many references may be found in the reviews of Brown and Weise,[23] Green,[24] and Weber and Arenhövel.[25] The pioneering work was by Sugawara and von Hippel[18] who attempted to make a zero-parameter NN potential. The fit to data was not very good, however, and the model was not used in nuclear structure calculations. In later work by Green and collaborators[26,27] only the transition $^1S_0(\mathrm{NN}) \leftrightarrow {}^5D_0(\mathrm{N}\Delta)$ was introduced; its addition to a modified Reid potential produced a significant saturating effect in nuclear matter, owing to dispersion and Pauli effects on the intermediate states. Additional channels were considered by Day and Coester,[28] while Holinde and Machleidt[29] modified their OBE models in such a way as to get effective NN interactions with the influence of $\Delta(1232)$ components built in. In both cases, a strong saturating effect in nuclear matter was observed. All these calculations used lowest-order Brueckner or lowest-order variational methods, however, which are no longer considered accurate.[30,31] They do not include the three-nucleon TPE attraction, while their dispersion corrections do include some of the three-nucleon repulsion.

Smith and Pandharipande[19] added $\mathrm{NN} \leftrightarrow \Delta\Delta$ transitions, which they found to be essential for the coupled-channels approach to make sense. They were able to get rough fits to S- and P-wave scattering data using only the iterated OPE potentials with $\pi N\Delta$ couplings for the intermediate-range attraction. The most complete

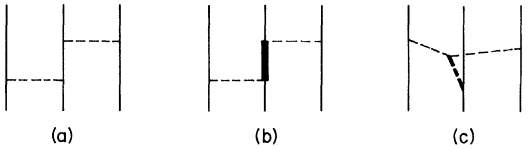

FIG. 2. Two-pion-exchange processes contributing to three-nucleon interaction; heavy dashed line in (c) represents ρ meson.

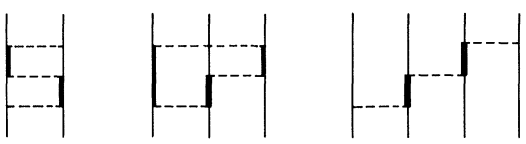

FIG. 4. Additional two-, three-, and four-nucleon interactions involving $\pi N\Delta$ coupling.

coupled-channels models to date are those of Niephaus, Gari, and Sommer.[32] They constructed several potentials with all possible $\pi N\Delta$ and $\pi\Delta\Delta$ couplings, plus ρNN, $\rho N\Delta$, and $\rho\Delta\Delta$ couplings. These were added to a modified Reid potential for the NN channels. Inexplicably, no repulsive core was added in the diagonal $N\Delta$ and $\Delta\Delta$ channels, which we believe is a serious drawback. If short-range repulsion is thought of as coming from ω exchange, then the repulsion in diagonal $N\Delta$ and $\Delta\Delta$ channels should be comparable to that in NN channels, since both quark and strong-coupling models indicate the coupling constant $f_{\omega\Delta\Delta}=f_{\omega NN}$.[33] Further, Wiringa[34] has found that in nuclear matter calculations where three-body clusters are considered, the lack of a repulsive core can lead to collapse, since two nucleons can come extremely close when one (or both) are excited to $\Delta(1232)$ states by transition correlations to a third nucleon. This effect is not apparent in lowest-order calculations[25] and the choice of diagonal interactions has little effect on fitting NN phase shifts.[19]

From this extensive body of work we draw several conclusions. The coupled-channels approach can be used to construct realistic NN potentials that make sense if $\Delta\Delta$ as well as $N\Delta$ intermediate states are included. Most of the intermediate-range attraction can be provided by the iterated OPE potential with $\pi N\Delta$ couplings, but some phenomenological portion should be left to allow for contributions from noniterative processes or higher resonances. A repulsive core should be present in the $N\Delta$ and $\Delta\Delta$ channels, comparable in strength to that in NN channels. Finally, to get the maximum benefit from such a potential, many-body calculations must include at least three-body clusters.

In this paper we present two new realistic NN potentials, Argonne v_{14} and Argonne v_{28}, so named for the location where the bulk of the numerical calculations were performed and their respective operator content. Argonne v_{14} is a conventional NN potential with 14 operator components and is similar in form to the Urbana[6] model. It is intended to serve as a standard of comparison for judging the effect of adding the $\Delta(1232)$, and has already been used in calculations of light nuclei and nuclear matter, with and without phenomenological three-nucleon potentials.[36] Argonne v_{28} has a v_{14} part for NN channels plus 14 transition and diagonal operators involving the $\Delta(1232)$. It embodies the key features described above, and is a logical and consistent extension of the v_{14}, in that the NN part has an identical form and the added OPE transition potentials have the same cutoff structure. The extra operators are so constrained that, aside from choices of $\pi N\Delta$ and $\pi\Delta\Delta$ coupling constants, there are no more free parameters for fitting data than in the v_{14}. The operator structure is particularly convenient for variational many-body calculations.

Particular attention has been paid to achieving a good description of NN data. Both models were fit to a 1981 phase shift analysis of Arndt and Roper[37] for np data in the range 25—400 MeV, plus deuteron properties and singlet np scattering length and effective range. A direct comparison to data was then made, and the χ^2 per data point was found to be comparable to that quoted for the parametrized Paris potential.[8] The two models are essentially phase equivalent, so that differences in the results of nuclear structure calculations should not be attributable to differences in their phase shifts.

The structure and parametrization of the v_{14} and v_{28} models is given in Secs. II and III, respectively. Details of the fitting procedure and a discussion of the phase-shift fits, deuteron properties, and data comparison are given in Sec. IV. A discussion of the resulting potentials and remarks about uses and possible future extensions of the models are given in Sec. V.

II. THE v_{14} POTENTIAL MODEL

The v_{14} potential is written as a sum of 14 operator components:

$$v_{14,ij}=\sum_{p=1,14}[v_\pi^p(r_{ij})+v_I^p(r_{ij})+v_S^p(r_{ij})]O_{ij}^p\ , \tag{1}$$

where the operators are

$$O_{ij}^{p=1,14}=1,\vec{\tau}_i\cdot\vec{\tau}_j,\vec{\sigma}_i\cdot\vec{\sigma}_j,(\vec{\sigma}_i\cdot\vec{\sigma}_j)(\vec{\tau}_i\cdot\vec{\tau}_j),S_{ij},S_{ij}(\vec{\tau}_i\cdot\vec{\tau}_j),(\vec{L}\cdot\vec{S}),(\vec{L}\cdot\vec{S})(\vec{\tau}_i\cdot\vec{\tau}_j),\vec{L}^2,\vec{L}^2(\vec{\tau}_i\cdot\vec{\tau}_j)\ ,$$
$$\vec{L}^2(\vec{\sigma}_i\cdot\vec{\sigma}_j),\vec{L}^2(\vec{\sigma}_i\cdot\vec{\sigma}_j)(\vec{\tau}_i\cdot\vec{\tau}_j),(\vec{L}\cdot\vec{S})^2,(\vec{L}\cdot\vec{S})^2(\vec{\tau}_i\cdot\vec{\tau}_j)\ . \tag{2}$$

Here

$$S_{ij}=3(\vec{\sigma}_i\cdot\hat{r}_{ij})(\vec{\sigma}_j\cdot\hat{r}_{ij})-\vec{\sigma}_i\cdot\vec{\sigma}_j$$

is the usual tensor operator, $\vec{L}$ is the relative orbital angular momentum, and $\vec{S}$ is the total spin of the pair. For convenience we will usually use the letters c, τ, σ, $\sigma\tau$, t, $t\tau$, b, $b\tau$, q, $q\tau$, $q\sigma$, $q\sigma\tau$, bb, and $bb\tau$ in referring to specific components.

The first eight operators of Eq. (2) are the standard ones required to fit singlet and triplet S- and P-wave data. The four L^2 operators provide for differences between S and D waves, and P and F waves. The $(L\cdot S)^2$ operators provide a third independent way [in addition to the S_{ij} and $(L\cdot S)$ operators] of splitting triplet states with different J values, e.g., ${}^3D_{1,2,3}$ states. These 14 operators provide sufficient freedom to characterize the 14 singlet and triplet S, P, D, and F states. This operator structure is identical to that in the Urbana[6] model, and has the same number of operators as the parametrized Paris[8] potentials.

The three radial components include the long-range OPE part $v_\pi^p(r)$, and phenomenological intermediate-range and short-range parts $v_I^p(r)$,$v_S^p(r)$, whose shapes are also taken from the Urbana model. The $v_\pi^p(r)$ contributes only with the $\sigma\tau$,$t\tau$ operators:

$$v_\pi^{\sigma\tau}(r)=\left[\frac{f_{\pi NN}^2}{4\pi}\frac{m_\pi}{3}\right]\frac{e^{-\mu r}}{\mu r}(1-e^{-cr^2})$$

$$\equiv(3.72681)Y_\pi(r)\ , \tag{3}$$

$$v_\pi^{t\tau}(r)=\left[\frac{f_{\pi NN}^2}{4\pi}\frac{m_\pi}{3}\right]\left[1+\frac{3}{\mu r}+\frac{3}{(\mu r)^2}\right]\frac{e^{-\mu r}}{\mu r}(1-e^{-cr^2})^2$$

$$\equiv(3.72681)T_\pi(r)\ . \tag{4}$$

$Y_\pi(r)$ and $T_\pi(r)$ are the usual Yukawa and tensor functions with smooth Gaussian cutoffs that make them vanish at $r=0$. The $(1-e^{-cr^2})^2$ cutoff in $T_\pi(r)$ was first used by Green and Haapakoski[26] and simulates the effect of ρ exchange, which we do not include explicitly. We take $c=2$ fm^{-2}, while the coefficient in brackets of $Y_\pi(r), T_\pi(r)$ is calculated using

$$(f_{\pi NN}^2/4\pi)=0.081$$

and

$$m_\pi=\tfrac{1}{3}(m_{\pi^0}+2m_{\pi^\pm})=138.03\ \text{MeV}\ .$$

The value of μ is calculated using $\hbar c=197.33$ MeV fm and the nucleon mass is taken as $m_N=\frac{1}{2}(m_n+m_p)=938.9$ MeV.

The intermediate-range parts $v_I^p(r)$ are assumed to come from TPE processes which will be dominated by the tensor interaction. Hence a reasonable phenomenological shape is

$$v_I^p(r)=I^pT_\pi^2(r)\ . \tag{5}$$

Finally, the short-range part is given a Woods-Saxon shape,

$$v_S^p(r)=S^p\{1+\exp[(r-R)/a]\}^{-1}\equiv S^pW(r)\ , \tag{6}$$

with $R=0.5$ fm, $a=0.2$ fm. The I^p and S^p are parameters to be determined by fitting data. Since there are 14 operators, there are 28 parameters; they are given in Table I. The values of the cutoff parameter c, and the Woods-Saxon parameters R and a have been taken from the Urbana model; since they gave very good fits to data, no attempt was made to alter them.

TABLE I. Potential strengths in operator channels (MeV) for the v_{14} model.

p	I^p	S^p
c	−4.801 125	2061.5625
τ	0.798 925	−477.3125
σ	1.189 325	−502.3125
$\sigma\tau$	0.182 875	97.0625
t	−0.1575	108.75
$t\tau$	−0.7525	297.25
b	0.5625	−719.75
$b\tau$	0.0475	−159.25
q	0.070 625	8.625
$q\tau$	−0.148 125	5.625
$q\sigma$	−0.040 625	17.375
$q\sigma\tau$	−0.001 875	−33.625
bb	−0.5425	391.0
$bb\tau$	0.0025	145.0

TABLE II. Potential strengths in singlet states (MeV) for the v_{14} model.

p	$I_{1,0}^p$	$S_{1,0}^p$	$I_{0,0}^p$	$S_{0,0}^p$
c	−8.1188	2800	−9.12	5874
q	0.05	63	0.62	−363

In practice, the potential components are obtained in their isospin and spin (T,S) projections, and then converted into the operator form of Eq. (1). In the T,S projection the singlet potentials are

$$v_{T,0}(r_{ij})=v_{\pi,T,0}(r_{ij})+\sum_{p=c,q}[I_{T,0}^pT_\pi^2(r_{ij})+S_{T,0}^pW(r_{ij})]O_{ij}^p\ , \tag{7}$$

and the triplet potentials are

$$v_{T,1}(r_{ij})=v_{\pi,T,1}(r_{ij})+\sum_{p=c,t,b,q,bb}[I_{T,1}^pT_\pi^2(r_{ij})+S_{T,1}^pW(r_{ij})]O_{ij}^p\ . \tag{8}$$

The different projections are related by

$$X_{T,S}^p=X^p+(4T-3)X^{p\tau}+(4S-3)X^{p\sigma}+(4S-3)(4T-3)X^{p\sigma\tau} \tag{9}$$

for $p=c,q$, and

$$X_{T,1}^p=X^p+(4T-3)X^{p\tau} \tag{10}$$

for $p=t$, b, and bb. The values of $I_{T,S}^p$ and $S_{T,S}^p$ are given in Tables II and III.

As stated above, the form of the v_{14} potential is similar to the Urbana[6] model. There are three differences between the Urbana and Argonne v_{14} models. First, the value for $f_{\pi NN}^2$ is ~7% larger than in the Urbana model, which contains the value used by Reid.[4] Second, we allow for short-range tensor components S^t and $S^{t\tau}$ in our force, whereas Urbana has $S^t=S^{t\tau}=0$. The Urbana choice here mimics the behavior of the parametrized Paris[8] potential, but we see no fundamental reason for this constraint. Third, probably as a result of relaxing this constraint, there is no need to introduce a second short-range Woods-Saxon function for $p=b,b\tau$ as in the Urbana model. The Argonne v_{14} phase shift fits are quite good with only one short-range functional shape. Aside from differences in phase shifts, which occur mostly at higher

TABLE III. Potential strengths in triplet states (MeV) for the v_{14} model.

p	$I_{0,1}^p$	$S_{0,1}^p$	$I_{1,1}^p$	$S_{1,1}^p$
c	−6.5572	2700	−2.63	1179
t	2.10	−783	−0.91	406
b	0.42	−242	0.61	−879
q	0.48	110	−0.12	−2
bb	−0.55	−44	−0.54	536

energies, the chief consequence of the changes above is a larger deuteron D state: 6.08% for Argonne v_{14} vs 5.2% for Urbana. The main reason for constructing a new v_{14} model is to have a phase-equivalent standard of comparison for the v_{28} model.

A nice feature of the Urbana model is the relatively small importance of $\vec{L}^2$ and $(\vec{L}\cdot\vec{S})^2$ ($O_{ij}^{p=9,14}$) terms, since their contribution to nuclear matter is calculated semiperturbatively when using variational wave functions and hypernetted chain techniques.[15] After obtaining our best fits to scattering data, we find this feature has been preserved in the Argonne v_{14} model. Nuclear matter calculations with Argonne v_{14} (Ref. 36) show that the ($O_{ij}^{p=9,14}$) contribute only $+1.8$ MeV per nucleon to the binding energy at $k_F=1.33$ fm^{-1}, the empirical saturation density, and $+6.1$ MeV at $k_F=1.6$ fm^{-1}. This contrasts with the parametrized Paris potential which, instead of the weak $\vec{L}^2$ terms, has strong $\vec{p}^{\,2}$ terms that contribute ~ -40 MeV per nucleon at $k_F=1.6$ fm^{-1}, for which our variational calculations may not be sufficiently accurate.[6]

III. THE v_{28} POTENTIAL MODEL

In the v_{28} model we start with a v_{14} part for NN channels, and add operators to represent all possible processes with πNΔ or $\pi\Delta\Delta$ vertices, plus central operators in the NΔ and $\Delta\Delta$ channels. The different kinds of processes are illustrated in Fig. 5. Because the N$\leftrightarrow\Delta$ transition involves a change of both spin and isospin from $\frac{1}{2}$ to $\frac{3}{2}$, each process involving a πNΔ vertex must have a spin-isospin or tensor-isospin operator, just as $v_\pi^p(r)$ contributes only to the $\sigma\tau$ and $t\tau$ parts of the NN channel, Fig. 5(a). Thus, two operators contribute to each of the transitions of Figs. 5(b)—(d) and (f). For the NΔ channel, Fig. 5(e), and $\Delta\Delta$ channel, Fig. 5(g), we use the two possible π-exchange operators plus a central operator, for a total of three each. The net result is a 28 component operator potential.

In analogy with Eq. (1) we write

$$v_{28,ij}=\sum_{p=1,28}[v_\pi^p(r_{ij})+v_I^p(r_{ij})+v_S^p(r_{ij})]O_{ij}^p\ , \tag{11}$$

where the $O_{ij}^{p=1,14}$ are given by Eq. (2) and the remaining operators are the following:

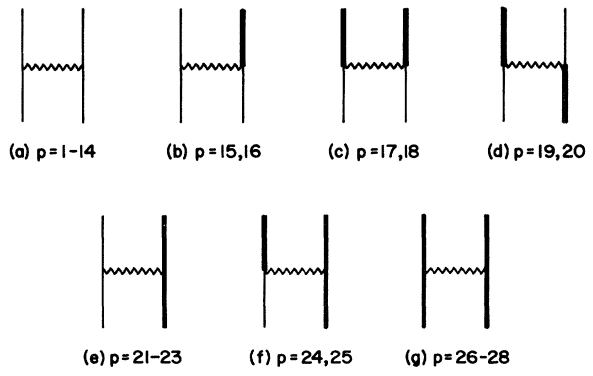

FIG. 5. Processes contained in the v_{28} potential model; numbers indicate which operators, O_{ij}^p, contribute to a given process.

$$O_{ij}^{p=15}=(\vec{\sigma}_i\cdot\vec{S}_j)(\vec{\tau}_i\cdot\vec{T}_j)+(\vec{S}_i\cdot\vec{\sigma}_j)(\vec{T}_i\cdot\vec{\tau}_j)$$
$$+\text{Hermitian conjugate (H.c.)}\ ,$$
$$O_{ij}^{16}=S_{ij}^{\rm II}(\vec{\tau}_i\cdot\vec{T}_j)+S_{ji}^{\rm II}(\vec{T}_i\cdot\vec{\tau}_j)+\text{H.c.}\ ,$$
$$O_{ij}^{17}=(\vec{S}_i\cdot\vec{S}_j)(\vec{T}_i\cdot\vec{T}_j)+\text{H.c.}\ ,$$
$$O_{ij}^{18}=S_{ij}^{\rm III}(\vec{T}_i\cdot\vec{T}_j)+\text{H.c.}\ ,$$
$$O_{ij}^{19}=(\vec{S}_i\cdot\vec{S}_j^{\,\dagger})(\vec{T}_i\cdot\vec{T}_j^{\,\dagger})+\text{H.c.}\ ,$$
$$O_{ij}^{20}=S_{ij}^{\rm IV}(\vec{T}_i\cdot\vec{T}_j^{\,\dagger})+\text{H.c.}\ ,$$
$$O_{ij}^{21}=1_{{\rm N}i}\cdot 1_{\Delta j}+1_{\Delta i}\cdot 1_{{\rm N}j}\ , \tag{12}$$
$$O_{ij}^{22}=(\vec{\sigma}_i\cdot\vec{\Sigma}_j)(\vec{\tau}_i\cdot\vec{\theta}_j)+(\vec{\Sigma}_i\cdot\vec{\sigma}_j)(\vec{\theta}_i\cdot\vec{\tau}_j)\ ,$$
$$O_{ij}^{23}=S_{ij}^{\rm V}(\vec{\tau}_i\cdot\vec{\theta}_j)+S_{ji}^{\rm V}(\vec{\theta}_i\cdot\vec{\tau}_j)\ ,$$
$$O_{ij}^{24}=(\vec{S}_i\cdot\vec{\Sigma}_j)(\vec{T}_i\cdot\vec{\theta}_j)+(\vec{\Sigma}_i\cdot\vec{S}_j)(\vec{\theta}_i\cdot\vec{T}_j)+\text{H.c.}\ ,$$
$$O_{ij}^{25}=S_{ij}^{\rm VI}(\vec{T}_i\cdot\vec{\theta}_j)+S_{ji}^{\rm VI}(\vec{\theta}_i\cdot\vec{T}_j)+\text{H.c.}\ ,$$
$$O_{ij}^{26}=1_{\Delta i}\cdot 1_{\Delta j}\ ,$$
$$O_{ij}^{27}=(\vec{\Sigma}_i\cdot\vec{\Sigma}_j)(\vec{\theta}_i\cdot\vec{\theta}_j)\ ,$$
$$O_{ij}^{28}=S_{ij}^{\rm VII}(\vec{\theta}_i\cdot\vec{\theta}_j)\ .$$

Here $\vec{S}_i$ ($\vec{T}_i$) is the transition spin (isospin) operator for particle i that changes a spin (isospin) $\frac{1}{2}$ state to a $\frac{3}{2}$ state, $\vec{\Sigma}_i$ ($\vec{\theta}_i$) is the Pauli spin (isospin) operator for a $\frac{3}{2}$ state, and $1_{{\rm N}i}$ ($1_{\Delta i}$) is the unit operator in N (Δ) space. [In this sense, the unit operator of Eq. (2), $O_{ij}^{p=1}=1_{{\rm N}i}\cdot 1_{{\rm N}j}$.] The various generalizations of the tensor operator S_{ij} are the following:

$$S_{ij}^{\rm II}=3(\vec{\sigma}_i\cdot\hat{r}_{ij})(\vec{S}_j\cdot\hat{r}_{ij})-\vec{\sigma}_i\cdot\vec{S}_j\ ,$$
$$S_{ij}^{\rm III}=3(\vec{S}_i\cdot\hat{r}_{ij})(\vec{S}_j\cdot\hat{r}_{ij})-\vec{S}_i\cdot\vec{S}_j\ ,$$
$$S_{ij}^{\rm IV}=3(\vec{S}_i\cdot\hat{r}_{ij})(\vec{S}_j^{\,\dagger}\cdot\hat{r}_{ij})-\vec{S}_i\cdot\vec{S}_j^{\,\dagger}\ , \tag{13}$$
$$S_{ij}^{\rm V}=3(\vec{\sigma}_i\cdot\hat{r}_{ij})(\vec{\Sigma}_j\cdot\hat{r}_{ij})-\vec{\sigma}_i\cdot\vec{\Sigma}_j\ ,$$
$$S_{ij}^{\rm VI}=3(\vec{S}_i\cdot\hat{r}_{ij})(\vec{\Sigma}_j\cdot\hat{r}_{ij})-\vec{S}_i\cdot\vec{\Sigma}_j\ ,$$
$$S_{ij}^{\rm VII}=3(\vec{\Sigma}_i\cdot\hat{r}_{ij})(\vec{\Sigma}_j\cdot\hat{r}_{ij})-\vec{\Sigma}_i\cdot\vec{\Sigma}_j\ .$$

For convenience, we may refer to $O_{ij}^{p=15-28}$ by the letters $\sigma\tau$II, $t\tau$II, $\sigma\tau$III, $t\tau$III, $\sigma\tau$IV, $t\tau$IV, cV, $\sigma\tau$V, $t\tau$V, $\sigma\tau$VI, $t\tau$VI, cVII, $\sigma\tau$VII, and $t\tau$VII. The explicit matrices for $\vec{\sigma}$, $\vec{S}$, and $\vec{\Sigma}$ are the following:

$$\vec{\sigma}=\begin{bmatrix}\hat{\epsilon}_0 & \sqrt{2}\hat{\epsilon}_-\\ -\sqrt{2}\hat{\epsilon}_+ & -\hat{\epsilon}_0\end{bmatrix}\ , \tag{14}$$

$$\vec{S}=\begin{bmatrix}-\hat{\epsilon}_- & 0\\ \sqrt{2/3}\hat{\epsilon}_0 & -\sqrt{1/3}\hat{\epsilon}_-\\ -\sqrt{1/3}\hat{\epsilon}_+ & \sqrt{2/3}\hat{\epsilon}_0\\ 0 & -\hat{\epsilon}_+\end{bmatrix}\ , \tag{15}$$

$$\vec{\Sigma}=\begin{bmatrix} 3\hat{\epsilon}_0 & \sqrt{6}\hat{\epsilon}_- & 0 & 0 \\ -\sqrt{6}\hat{\epsilon}_+ & \hat{\epsilon}_0 & \sqrt{8}\hat{\epsilon}_- & 0 \\ 0 & -\sqrt{8}\hat{\epsilon}_+ & -\hat{\epsilon}_0 & \sqrt{6}\hat{\epsilon}_- \\ 0 & 0 & -\sqrt{6}\hat{\epsilon}_+ & -3\hat{\epsilon}_0 \end{bmatrix}, \quad (16)$$

where $\hat{\epsilon}_\pm=\mp\sqrt{1/2}(\hat{x}\pm i\hat{y})$, $\hat{\epsilon}_0=\hat{z}$. The reduced matrix elements are (using Edmonds's convention)[38]:

$$(\tfrac{1}{2}||\vec{\sigma}||\tfrac{1}{2})=\sqrt{6}\,, \quad (17)$$

$$(\tfrac{3}{2}||\vec{S}||\tfrac{1}{2})=-(\tfrac{1}{2}||\vec{S}^\dagger||\tfrac{3}{2})=2\,, \quad (18)$$

$$(\tfrac{3}{2}||\vec{\Sigma}||\tfrac{3}{2})=2\sqrt{15}\,. \quad (19)$$

The set of transition operators in Eq. (12) cannot be enlarged without introducing momentum dependence. However, there could be many more diagonal operators in the NΔ and ΔΔ channels, including spin, isospin, tensor, and spin-orbit components. Unfortunately, low-energy NN scattering data does not give us much information on this, and our only guide is the theoretical expectation that there should be a repulsive core comparable to that in NN channels. For the sake of simplicity we have added only central operators to those required by OPE processes. Further, we will assume that only $v_\pi^p(r)$ contributes to the transition parts of the potential, i.e., $v_I^p(r)=v_S^p(r)\equiv 0$ for $p=15$–20, 24, and 25. For the NΔ and ΔΔ channels we do the same for the spin-isospin and tensor-isospin operators, $p=22$, 23, 27, and 28. The only new nonzero $v_I^p(r)$ and $v_S^p(r)$ will be for the central operators in NΔ and ΔΔ channels, $p=21,26$.

The $v_\pi^p(r)$ of Eq. (11) representing OPE thus contributes to all the $O_{ij}^{p=15-28}$ except for cV and cVII. The only change from Eqs. (3) and (4) is in the need to substitute appropriate combinations of the coupling constants $f_{\pi\mathrm{NN}}$, $f_{\pi\mathrm{N}\Delta}$, and $f_{\pi\Delta\Delta}$. Unfortunately the latter two are not well determined. Sugawara and von Hippel[18] obtained $(f_{\pi\mathrm{N}\Delta}^2/4\pi)=0.35$ by equating the first order expression for the Δ decay width with the experimental width. The value equivalent to the Chew-Low theory,[23] is

$$(f_{\pi\mathrm{N}\Delta}^2/4\pi)=4(f_{\pi\mathrm{NN}}^2/4\pi)=0.324\,,$$

while the strong-coupling model (see Appendix 2 of Ref. 24) has

$$(f_{\pi\mathrm{N}\Delta}^2/4\pi)=(9/2)(f_{\pi\mathrm{NN}}^2/4\pi)=0.365\,.$$

However, the quark model gives only

$$(f_{\pi\mathrm{N}\Delta}^2/4\pi)=(72/25)(f_{\pi\mathrm{NN}}^2/4\pi)=0.233\,.^{23}$$

Niskanen[39] has recently argued that higher-order mesonic effects can explain the difference between the quark and experimental values. We feel an "effective" $f_{\pi\mathrm{N}\Delta}$ is appropriate here, close to the experimental value, and since four is a nice round number, we arbitrarily take the Chew-Low value,

$$(f_{\pi\mathrm{N}\Delta}^2/4\pi)=4(f_{\pi\mathrm{NN}}^2/4\pi)=0.324\,.$$

For the $\pi\Delta\Delta$ vertex we have no experimental information. Fortunately, both the quark and strong-coupling models are in agreement, with

TABLE IV. Potential strengths in operator channels (MeV) for the v_{28} model.

p	I^p	S^p
c	−2.2	1960
τ	1.652 225	−770.5
σ	0.786 425	−311.75
$\sigma\tau$	0.083 150	118.25
t	0.105	62.75
$t\tau$	−0.945	505.25
b	0.71	−912.5
$b\tau$	−0.05	−136.5
q	0.191 875	−23.875
$q\tau$	−0.106 875	−17.375
$q\sigma$	0.013 125	−24.875
$q\sigma\tau$	0.001 875	−38.875
bb	−0.7425	531.75
$bb\tau$	−0.0675	188.25

$$(f_{\pi\Delta\Delta}^2/4\pi)=(1/25)(f_{\pi\mathrm{NN}}^2/4\pi)=0.003\,24\,.$$

Thus we take

$$v_\pi^{\sigma\tau x}(r)=\left[\frac{f^2}{4\pi}\frac{m_\pi}{3}\right]_x Y_\pi(r)\,, \quad (20)$$

$$v_\pi^{t\tau x}(r)=\left[\frac{f^2}{4\pi}\frac{m_\pi}{3}\right]_x T_\pi(r)\,, \quad (21)$$

where $Y_\pi(r)$ and $T_\pi(r)$ are given by Eqs. (3) and (4), and

$$\left[\frac{f^2}{4\pi}\frac{m_\pi}{3}\right]_x \begin{cases} =7.45362\ (x=\mathrm{II})\,, \\ =14.90724\ (\mathrm{III,IV})\,, \\ =0.745362\ (\mathrm{V})\,, \\ =1.490724\ (\mathrm{VI})\,, \\ =0.1490724\ (\mathrm{VII})\,. \end{cases} \quad (22)$$

The only remaining new operators are $p=c$V and cVII, which we will require to equal the central NN operator:

$$v_I^{c\mathrm{V}}(r)=v_I^{c\mathrm{VII}}(r)=v_I^c(r)\equiv I^c T_\pi^2(r)\,, \quad (23)$$

$$v_S^{c\mathrm{V}}(r)=v_S^{c\mathrm{VII}}(r)=v_S^c(r)\equiv S^c W(r)\,. \quad (24)$$

where $W(r)$ is defined by Eq. (6).

Having fixed the strengths and shapes of all the transition potentials and the NΔ and ΔΔ channels, the only remaining task is to redetermine the 28 coefficients $I^{p=1,14}$, $S^{p=1,14}$ by fitting phase shifts and deuteron properties. These coefficients are given in Table IV, and the (T,S) projections are given in Tables V and VI.

TABLE V. Potential strengths in singlet states (MeV) for the v_{28} model.

p	$I_{1,0}^p$	$S_{1,0}^p$	$I_{0,0}^p$	$S_{0,0}^p$
c	−3.1565	1770	−8.7676	6271
q	0.04	150	0.49	−247

TABLE VI. Potential strengths in triplet states (MeV) for the v_{28} model

p	$I^p_{0,1}$	$S^p_{0,1}$	$I^p_{1,1}$	$S^p_{1,1}$
c	−6.6197	3605	0.3218	996
t	2.94	−1453	−0.84	568
b	0.86	−503	0.66	−1049
q	0.52	120	0.10	−105
bb	−0.54	−33	−0.81	720

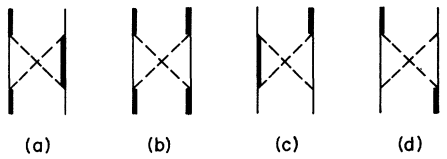

FIG. 6. Cross-box two-pion-exchange processes that could contribute to (a) NΔ and (b) ΔΔ interactions, and (c) and (d) transitions.

Although a number of arbitrary decisions have been made regarding the choice and shape of the new operators, we believe the essential features have been added with simplicity and consistency. All allowed OPE couplings are included, plus a repulsive core in the NΔ and ΔΔ channels. The ρ meson has not been added, but its major effect of reducing the OPE tensor at short distances is still included by the cutoff in $T_\pi(r)$. [Explicit addition of ρNΔ and $\rho\Delta\Delta$ couplings would require only two new operators, $(\vec{\tau}_i\cdot\vec{\theta}_j)$ and $(\vec{\theta}_i\cdot\vec{\theta}_j)$, coming from the relatively weak vector coupling.] Retention of the $v_l^p(r)$ terms in the NN channel should simulate to some extent the crossed-box TPE diagrams [Figs. 1(d)—(f)] which are not included explicitly; the strength of these terms is determined by how much is still required to fit the data. The inclusion of $v_l^{c\,\mathrm{V}}(r)$ and $v_l^{c\,\mathrm{VII}}(r)$ is attributed to crossed-box diagrams in the NΔ and ΔΔ channels, as illustrated in Figs. 6(a) and (b), although it is also only an approximate replacement.

IV. PHASE SHIFT FITTING AND COMPARISON TO DATA

The full Hamiltonian is a sum of rest-mass and kinetic energy operators and the interaction given by Eq. (1) for v_{14} or Eq. (11) for v_{28}. Since it is invariant under rotations, reflections, and isospin rotations, the two-body problem can be solved separately for each set of channels with definite angular momentum J, parity P, and isospin T. In general, a number of NN, NΔ, and ΔΔ states described by various values of angular momentum L and spin S adding up to J are coupled through the interaction term. The allowed states for $J\leq 5$ are shown in Table VII; all were used in the present work. For each J^P,T the Hamiltonian may be written as a small matrix which couples these different states. Schematically, the Schrödinger equation may be written as

$$\sum_j H_{ij}\psi_j = E\psi_i \ , \tag{25}$$

where in the center of mass frame

$$H_{ij} = (m_i + m_j - 2m_{\mathrm{N}}) + \frac{\hbar^2(m_i+m_j)}{2m_i m_j}\nabla^2_{ij} + V_{ij} \ . \tag{26}$$

The matrix elements of the potential operators are computed through standard angular momentum algebra, as in Edmonds's convention.[38] The result for spin-spin operators is

$$\langle s_1' s_2' S' \,|\, \vec{\mathrm{s}}_1\cdot\vec{\mathrm{s}}_2 \,|\, s_1 s_2 S\rangle = (-1)^{s_1+s_2'+S}\delta_{SS'}\begin{Bmatrix} S & s_2' & s_1' \\ 1 & s_1 & s_2 \end{Bmatrix}(s_1'||\vec{\mathrm{s}}_1||s_1)(s_2'||\vec{\mathrm{s}}_2||s_2) \ , \tag{27}$$

where $\vec{\mathrm{s}}_1$ and $\vec{\mathrm{s}}_2$ can be any of the operators $\vec{\sigma}$, $\vec{\mathrm{S}}$, and $\vec{\Sigma}$, and the reduced matrix elements are those of Eqs. (17)—(19). This expression also applies to the corresponding isospin-isospin matrix elements. For the tensor operators S^x_{12} of Eq. (13) the matrix elements are

$$\langle L'(s_1' s_2' S')J \,|\, S^x_{12}(\vec{\mathrm{s}}_1,\vec{\mathrm{s}}_2) \,|\, L(s_1 s_2 S)J\rangle = (-1)^{S'+J}[30(2L+1)(2S+1)(2L'+1)(2S'+1)]^{1/2}\begin{Bmatrix} J & S' & L' \\ 2 & L & S \end{Bmatrix}\begin{Bmatrix} L' & 2 & L \\ 0 & 0 & 0 \end{Bmatrix}$$
$$\times\begin{Bmatrix} s_1' & s_1 & 1 \\ s_2' & s_2 & 1 \\ S' & S & 2 \end{Bmatrix}(s_1'||\vec{\mathrm{s}}_1||s_1)(s_2'||\vec{\mathrm{s}}_2||s_2) \ . \tag{28}$$

These expressions are in agreement with those of Refs. 19 and 32. Because an NΔ channel and the corresponding ΔN channel wave functions differ at most by a phase, it suffices to multiply the coupling of these channels by $\sqrt{2}$ and keep only one channel in the calculation. This requires some care in looking at the matrix elements of ΔN-NΔ transition operators. The only other matrix elements needed are the spin-orbit and $\vec{\mathrm{L}}^2$ operators of Eq. (2) which appear in NN channels; their calculation is straightforward.

For the deuteron, the Schrödinger equation is to be solved as an eigenvalue problem for the binding energy $-E$; the resulting eigenfunctions can be used to calculate other deuteron properties. For computing phase shifts, the energy is prescribed and the asymptotic forms of NN wave functions are used to obtain the phase shifts. As

TABLE VII. NN, NΔ, and ΔΔ partial waves ($^{2S+1}L_J$) used in this work.

NN	NΔ	ΔΔ
$^1S_0$	$^5D_0$	$^1S_0{}^5D_0$
$^1D_2$	$^5S_2{}^3D_2{}^5D_2{}^5G_2$	$^5S_2{}^1D_2{}^5D_2{}^5G_2$
$^1G_4$	$^5D_4{}^3G_4{}^5G_4{}^5I_4$	$^5D_4{}^1G_4{}^5G_4{}^5I_4$
$^3P_0$	$^3P_0$	$^3P_0{}^7F_0$
$^3P_1$	$^3P_1{}^5P_1{}^5F_1$	$^3P_1{}^7F_1$
$^3P_2$-$^3F_2$	$^3P_2{}^5P_2{}^3F_2{}^5F_2$	$^3P_2{}^7P_2{}^3F_2{}^7F_2{}^7H_2$
$^3F_3$	$^5P_3{}^3F_3{}^5F_3{}^5H_3$	$^7P_3{}^3F_3{}^7F_3{}^7H_3$
$^3F_4$-$^3H_4$	$^3F_4{}^5F_4{}^3H_4{}^5H_4$	$^7P_4{}^3F_4{}^7F_4{}^3H_4{}^7H_4{}^7K_4$
$^3H_5$	$^5F_5{}^3H_5{}^5H_5{}^5K_5$	$^7F_3{}^3H_5{}^7H_5{}^7K_5$
$^3S_1$-$^3D_1$		$^3S_1{}^3D_1{}^7D_1{}^7G_1$
$^3D_2$		$^3D_2{}^7D_2{}^7G_2$
$^3D_3$-$^3G_3$		$^7S_3{}^3D_3{}^7D_3{}^3G_3{}^7G_3{}^7I_3$
$^3G_4$		$^7D_4{}^3G_4{}^7G_4{}^7I_4$
$^3G_5$-$^3I_5$		$^7D_5{}^3G_5{}^7G_5{}^3I_5{}^7I_5{}^7L_5$
$^1P_1$		$^1P_1{}^5P_1{}^5F_1$
$^1F_3$		$^5P_3{}^1F_3{}^5F_3{}^5H_3$
$^1H_5$		$^5F_5{}^1H_5{}^5H_5{}^5K_5$

long as the energy is not high enough to produce a real Δ, the NΔ and ΔΔ channels decay exponentially at large distances. At small distances, r times the wave function in any channel goes to zero at the origin. The couplings to NΔ or ΔΔ channels are ignored beyond a separation of 7 fm.

We solve the deuteron by integrating the set of six coupled equations outward from the origin using six independent sets of initial slopes. We also integrate the six equations inward from large r (15 fm) using another six independent sets of initial values, with logarithmic derivatives obtained assuming a specific value for the binding energy. Linear combinations of the inner and outer solutions are then matched at an intermediate distance, such that all wave functions are continuous and all first derivatives except the $^3S_1$ NN derivative are continuous there. The assumed binding energy is then varied to make this continuous also. A few iterations usually suffice. This method is similar to that used by Gari, Hyuga, and Sommer.[40]

The phase-shift problem is treated slightly differently according to whether there are one or two NN channels. In either case the complete set of n channels is integrated outward with n independent choices of initial slope to a maximum value of r (15 fm). Linear combinations of these are taken in which all of the NΔ and ΔΔ channels vanish asymptotically. If one NN channel remains, its asymptotic form is found and used to compute the phase shift. If two NN channels remain, they are used to compute the S matrix. With the assumption that the mixing angle is small, this leads to an unambiguous identification of the phase-shift parameters.

The potentials were fitted to the np phase-shift analysis WI81 of Arndt and Roper[37] in all partial waves for $J \leq 5$ up to 400 MeV. We used the energy-dependent values with the energy-independent error bars as our constraint. In addition, we fitted the deuteron binding energy E_d,[41] quadrupole moment Q_d,[42] and asymptotic ratio of D- and S-state amplitudes η_d,[43] and the singlet np scattering length $^1a_{np}$ and effective range $^1r_{np}$.[44] These quantities serve particularly to fix the low-energy $^3S_1$-$^3D_1$ and $^1S_0$ properties. Fitting np data avoids the necessity of considering Coulomb effects. It also has advantages for studying deuteron interactions such as n(p,γ)d and d(γ,p)n.

To search effectively for the 28 I^p and S^p parameters, we used the T,S projection of Eqs. (7) and (8). We computed the phase shifts of all partial waves with specified T,S at seven energies from 25 to 400 MeV plus any appropriate low-energy properties for a given set of input parameters: four parameters in singlet states and ten in triplet states. A minimization routine based on the Levenberg-Marquardt algorithm, LMDIF,[45] was then used to adjust the parameters to obtain the best χ^2 fit to the data. For example, in $T=1,S=0$ states we varied $I^c_{1,0}$, $I^q_{1,0}$, $S^c_{1,0}$, and $S^q_{1,0}$ to fit seven phase shifts each in $^1S_0$, $^1D_2$, and $^1G_4$ partial waves, plus the values for $^1a_{np}$, $^1r_{np}$—a total of 23 data points.

The Urbana model provided good initial guesses for the Argonne v_{14} model, which in turn helped initiate the search in the v_{28} model. In the latter case, a guess had to be made for the I^c,S^c parameters which specify the core interaction in NΔ and ΔΔ channels. Then the best fits in all channels were obtained and the actual I^c,S^c were projected out. The fitting procedure was then repeated with the new values. The fits are not very sensitive to details of the core in the NΔ and ΔΔ channels, and three iterations were sufficient to get convergence.

The phase shifts for $J \leq 4$ are shown in Figs. 7–13. The dots with error bars are the WI81 energy-independent

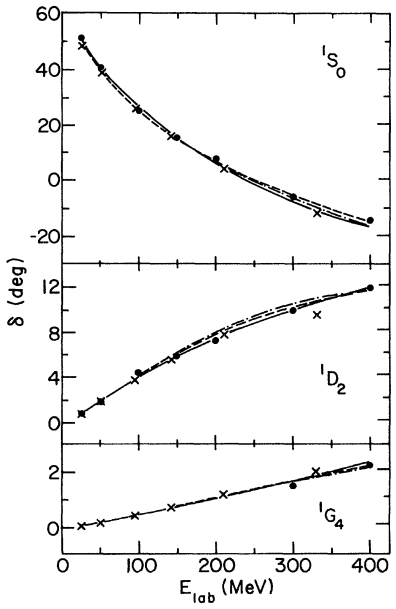

FIG. 7. $T=1,S=0$ phase shifts: solid lines and dots with error bars are the energy-dependent and energy-independent phases of Arndt and Roper (Ref. 37), solution WI81; dash-dot and dashed lines are v_{14} and v_{28} model phases, respectively, while crosses show parametrized Paris (Ref. 8) phases.

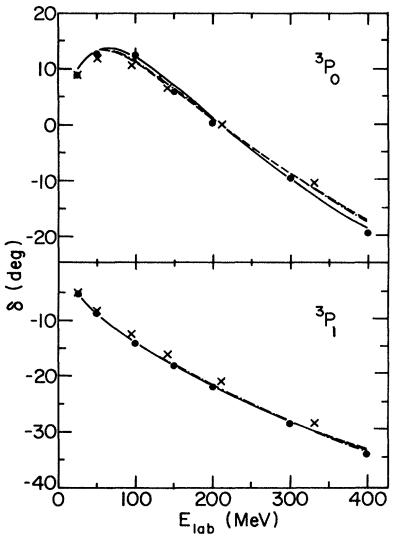

FIG. 8. $T=1, S=1$ phase shifts: notation as in Fig. 7.

values of Arndt and Roper,[37] while the solid lines are the energy-dependent values. The dash-dot lines show the v_{14} phase shifts and the dashed lines show v_{28}. For comparison the parametrized Paris[8] phase shifts are shown as $\times$'s; it should be noted that the Paris group chose to fit pp phase shifts in $T=1$ states. The models reproduce the phase shifts well in all channels except $^3H_4$; the lack of any energy-independent values there makes it hard to judge the importance of that channel. In most channels the v_{14} and v_{28} models reproduce the experimental phase shifts as well as the parametrized Paris model, and in some channels, such as $^1P_1$ and $^3D_2$, they seem better. The similarity of the v_{14} and v_{28} phase shifts shows how close they are to being phase equivalent.

As the Paris group has emphasized, a more rigorous test of the quality of the fits is to compare the potential

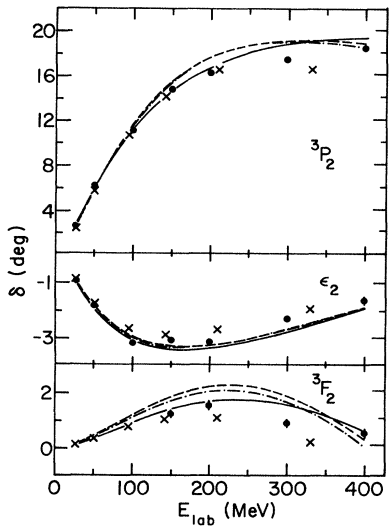

FIG. 9. $T=1, S=1$ phase shifts: notation as in Fig. 7.

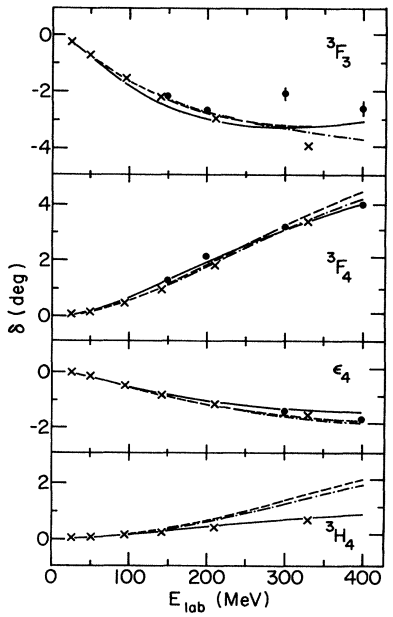

FIG. 10. $T=1, S=1$ phase shifts: notation as in Fig. 7.

predictions directly to data. We did this by calculating phase shifts at 14 energies from 10 to 325 MeV for all $J \leq 5$ partial waves and using the SAID program of Arndt and Roper[37] to compute a variety of observables and make a χ^2 comparison to a large data base. We compared our predictions with all the np data between 5 and 330 MeV in the 1982 SAID data base. For 1762 points, including total cross sections, differential cross sections, polarizations, etc., we obtained a χ^2 of 2889 for v_{14} and 2990 for v_{28}, or a χ^2 per point of 1.64 and 1.70, respectively. Thus the quality of our fit is excellent. The Paris group quotes a χ^2

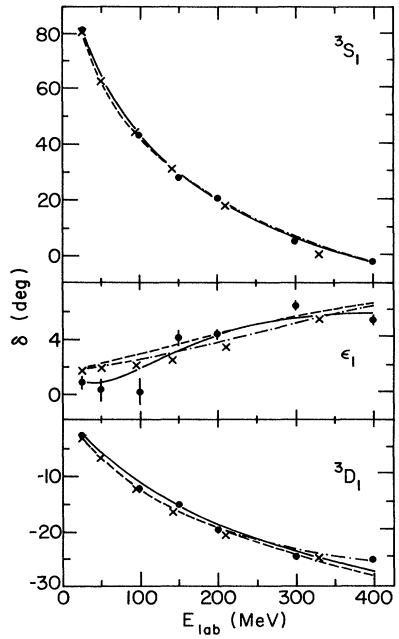

FIG. 11. $T=0, S=1$ phase shifts: notation as in Fig. 7.

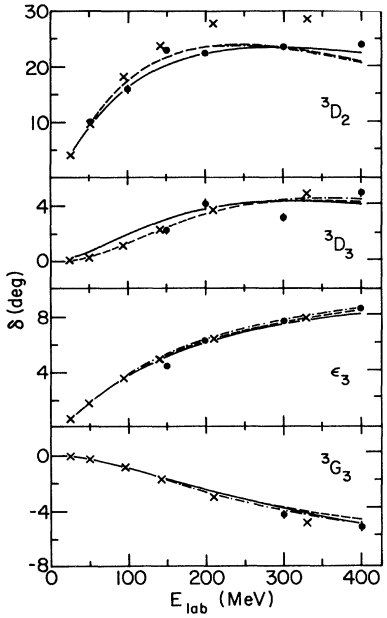

FIG. 12. $T=0,S=1$ phase shifts: notation as in Fig. 7.

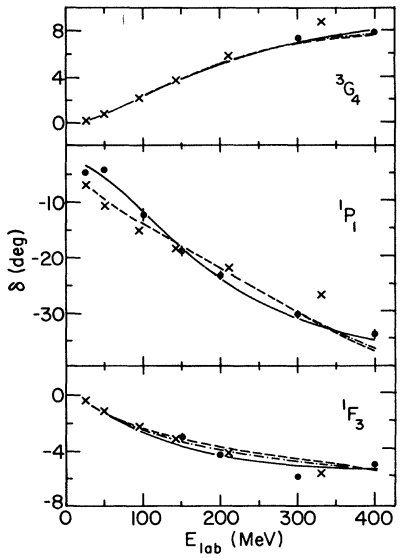

FIG. 13. $T=0,S=1$ and $T=0,S=0$ phase shifts: notation as in Fig. 7.

per point of 2.17 for np data,[8] but they have obviously used a different (and larger) data base, so direct comparison of these figures is not possible.

The fitted deuteron and low-energy scattering quantities are shown in Table VIII, along with experimental values[41–44] and Paris predictions. Also shown are the calculated deuteron D-state and Δ-state percentages P_D, P_Δ and magnetic moment μ_d, and the triplet scattering parameters, which we did not attempt to fit. For the v_{28} model, the total P_Δ of 0.52% breaks down into components: $P_\Delta(^3S_1)=0.04\%$, $P_\Delta(^3D_1)=0.02\%$, $P_\Delta(^7D_1)=0.42\%$, and $P_\Delta(^7G_1)=0.04\%$. The deuteron wave functions are shown in Fig. 14 and the deuteron form factor $A(q^2)$ is shown in Fig. 15. In both figures, the dashed, solid, and dotted lines show, respectively, the v_{14}, v_{28}, and parametrized Paris values; experimental data for $A(q^2)$ is from Galster *et al.*[46] and references therein.

The form factor is given by a sum of charge, quadrupole, and magnetic parts[47]

$$A(q^2)=G_0(q^2)+\tfrac{8}{9}\eta^2 G_2^2(q^2)+\tfrac{2}{3}\eta G_1^2(q^2)\,, \tag{29}$$

where $\eta=q^2/4m_d^2$, m_d is the deuteron mass, and in impulse approximation

$$G_0(q^2)=2G_E^s(q^2)\int dr\, j_0(\tfrac{1}{2}qr)(u_{01}^2+u_{21}^2+\tilde{u}_{01}^2+\tilde{u}_{21}^2+\tilde{u}_{23}^2+\tilde{u}_{43}^2)\,, \tag{30}$$

$$\eta G_2(q^2)=2G_E^s(q^2)\int dr\, j_2(\tfrac{1}{2}qr)\left[\frac{3}{\sqrt{2}}u_{01}u_{21}-\tfrac{3}{4}u_{21}^2+\frac{3}{\sqrt{2}}\tilde{u}_{01}\tilde{u}_{21}-\tfrac{3}{4}\tilde{u}_{21}^2-\tfrac{3}{14}\tilde{u}_{23}^2+\frac{9\sqrt{3}}{7}\tilde{u}_{23}\tilde{u}_{43}-\tfrac{15}{28}\tilde{u}_{43}^2\right], \tag{31}$$

TABLE VIII. The calculated deuteron and low-energy parameters.

	v_{14}	v_{28}	Paris[a]	Experiment
E_d (MeV)	−2.2250	−2.2250	−2.2249	−2.224 63(3)
Q_d (fm^2)	0.286	0.286	0.279	0.2860(15)
η_d	0.0266	0.0265	0.0261	0.0265(5)
μ_d (μ_N)	0.845	0.846	0.853	0.857 441(2)
P_D (%)	6.08	6.13	5.77	4–7
P_Δ (%)	0	0.52	0	?
$^3a_{np}$ (fm)	5.45	5.46	5.427	5.424(4)
$^3r_{np}$ (fm)	1.80	1.81	1.766	1.748(6)
$^1a_{np}$ (fm)	−23.67	−23.70	b	−23.715(15)
$^1r_{np}$ (fm)	2.77	2.78	b	2.73(3)

[a]Values reported in Ref. 8.
[b]Not published in Ref. 8.

$$\frac{m_N}{m_d}G_1(q^2)=G_E^s(q^2)\int dr[j_0(\tfrac{1}{2}qr)+j_2(\tfrac{1}{2}qr)][\tfrac{3}{2}u_{21}^2+\frac{m_N}{m_\Delta}(\tfrac{3}{2}\tilde{u}_{21}^2-\tilde{u}_{23}^2+\tfrac{5}{2}\tilde{u}_{43}^2)]$$

$$+2G_M^s(q^2)\int dr\left[j_0(\tfrac{1}{2}qr)(u_{01}^2-\tfrac{1}{2}u_{21}^2+\tilde{u}_{01}^2-\tfrac{1}{2}\tilde{u}_{21}^2+2\tilde{u}_{23}^2-\tfrac{3}{2}\tilde{u}_{43}^2)\right.$$

$$\left.+j_2(\tfrac{1}{2}qr)\left[\frac{1}{\sqrt{2}}u_{01}u_{21}+\tfrac{1}{2}u_{21}^2+\frac{1}{\sqrt{2}}\tilde{u}_{01}\tilde{u}_{21}+\tfrac{1}{2}\tilde{u}_{21}^2-\tfrac{4}{7}\tilde{u}_{23}^2+\frac{3\sqrt{3}}{7}\tilde{u}_{23}\tilde{u}_{43}+\tfrac{15}{4}\tilde{u}_{43}^2\right]\right]. \quad (32)$$

Here $u_{LS},\tilde{u}_{LS}$ denote the NN and $\Delta\Delta$ components of the wave function, and $G_E^s(q^2),G_M^s(q^2)$ are the isoscalar electric and magnetic form factors for the nucleons, normalized as $G_E^s(0)=\frac{1}{2}$, $G_M^s(0)=\frac{1}{2}(\mu_p+\mu_n)$. In the limit $q\to 0$, the quadrupole moment is given by $Q_d=G_2(0)/m_d^2$ and the magnetic moment by $\mu_d=G_1(0)m_N/m_d$. The factors associated with the $\tilde{u}_{LS}$ agree with those found by Gari, Hyuga, and Sommer,[40] and in the $q=0$ limit with the factors found by Hadjimichael[48] for the static moments. However, we disagree with the latter's remarks about the isoscalar magnetic moment for the $\Delta\Delta$ components; we find the $G_M^s(0)$ for nucleons is consistent with the simple quark model for Δ structure and the restrictions on how the Δ couples in $\tilde{u}_{LS}$. We agree with the $q=0$ limit of Ref. 40, and we believe the use of the same $G_E^s(q^2),G_M^s(q^2)$ for Δ components as for nucleons is reasonable. For the $A(q^2)$ shown in Fig. 15, we use the form factors from fit 8.2 of Höhler *et al.*[49] with their $m_\omega=0.784$ GeV, $m_\phi=1.02$ GeV.

All the fitted quantities in Table VIII are well reproduced, but μ_d (Ref. 50) is not. The $A(q^2)$ also agrees well with the experimental data. We note there should be additional contributions to the static moments and form factors from meson exchange currents[40,48] and relativistic corrections[51] which we have not attempted to calculate. Such contributions could easily account for the difference between the calculated and experimental μ_d, but might well destroy the nice agreement for Q_d, while changes in $A(q^2)$ might be as large as 10% for some values of q. The D-state percentage is higher for the v_{14} and v_{28} models than for Urbana or parametrized Paris models. Arenhövel and Fabian[52] have argued that a smaller tensor force, which is frequently characterized by P_D, would better explain the forward cross section data for d(γ,p)n. However, recent work by Cambi *et al.*[53] and Hwang *et al.*[54] suggests that other explanations may be possible. Having picked the general functional form for our potential models, our P_D, Q_d, η_d, and μ_d are determined primarily by the fit to phase-shift data and deuteron binding energy.

V. DISCUSSION

The $v_{T,S}^p(r)$ are shown in Figs. 16–21, with dashed lines for the v_{14} model and solid lines for the v_{28} model. For convenience we will refer to components of the v_{14} and v_{28} models as $v_{T,S}^p$ and $\tilde{v}_{T,S}^p$, respectively. The main effect of explicitly introducing $\Delta(1232)$ degrees of freedom in the NN potential is to reduce the amount of intermediate range attraction in NN channels required by the data. This is because the effective interaction, $V_{\rm eff}$, provided by the (predominantly) tensor couplings to NΔ and $\Delta\Delta$ intermediate states is large and attractive. This can be seen in the simple closure approximation[19,26]

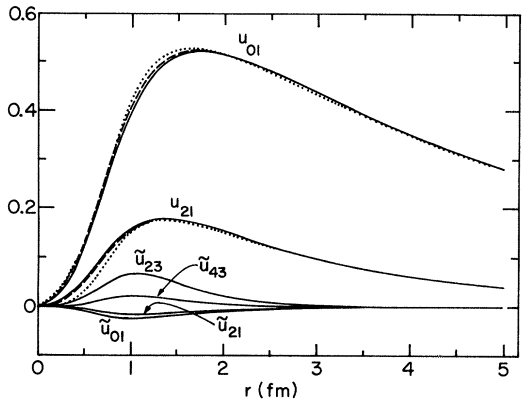

FIG. 14. Deuteron wave functions: solid, dashed, and dotted lines give v_{28}, v_{14}, and parametrized Paris results.

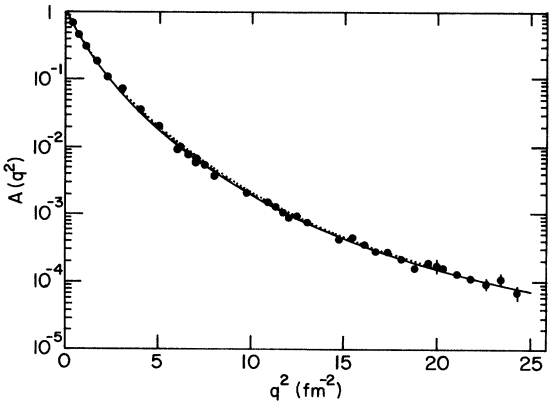

FIG. 15. Deuteron form factor $A(q^2)$: solid, dashed, and dotted lines give v_{28}, v_{14}, and parametrized Paris results; experimental results from Galster *et al.* (Ref. 46) and references therein.

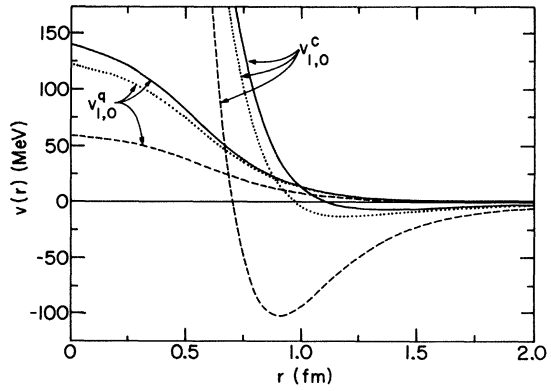

FIG. 16. $T=1,S=0$ central and $\vec{L}^2$ potentials: solid and dashed lines show v_{28} and v_{14} models; dotted lines show potentials for a v_{21} model with NN and NΔ but no ΔΔ channels.

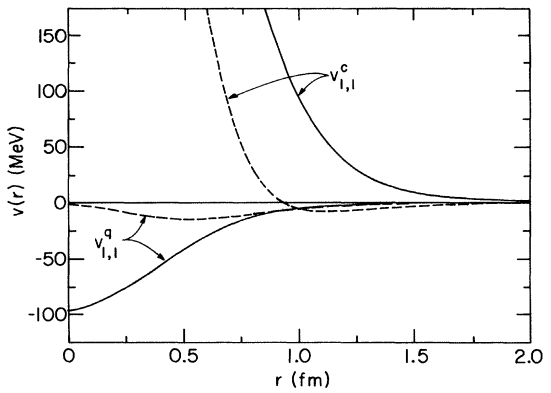

FIG. 18. $T=1,S=1$ central and $\vec{L}^2$ potentials: solid and dashed lines show v_{28} and v_{14} models.

$$V_{\text{eff}} \approx -\left[2\left[\frac{f_{\pi NN} f_{\pi N\Delta}}{4\pi}\frac{m_\pi}{3}\right]^2 \frac{(\vec{\tau}_i\cdot\vec{T}_j^{\dagger})(\vec{\tau}_i\cdot\vec{T}_j)S_{ij}^{II\dagger}S_{ij}^{II}}{\bar{E}+(m_\Delta-m_N)} + \left[\frac{f^2_{\pi N\Delta}}{4\pi}\frac{m_\pi}{3}\right]^2 \frac{(\vec{T}_i^{\dagger}\cdot\vec{T}_j^{\dagger})(\vec{T}_i\cdot\vec{T}_j)S_{ij}^{III\dagger}S_{ij}^{III}}{\bar{E}+2(m_\Delta-m_N)}\right] T_\pi^2(r)$$

$$= -[1.85+0.25\vec{\tau}_i\cdot\vec{\tau}_j - 0.126(\vec{\sigma}_i\cdot\vec{\sigma}_j - S_{ij}) - 0.072(\vec{\sigma}_i\cdot\vec{\sigma}_j - S_{ij})\vec{\tau}_i\cdot\vec{\tau}_j]T_\pi^2(r)\,, \tag{33}$$

where we have set the mean energy denominator, $\bar{E}=500$ MeV. This attraction will be greatest (~ 100 MeV at $r=1$ fm) in $T=1,S=0$ states, somewhat less in $T=1,S=1$ and $T=0,S=1$ states, and least (~ 30 MeV at $r=1$ fm) in $T=0,S=0$ states. The $\tilde{v}^c_{T,S}$ must be correspondingly less attractive than $v^c_{T,S}$ to produce the same phase shifts. This is indeed the case, as can be seen in Figs. 16–19. We also expect $\tilde{v}^t_{1,1} > v^t_{1,1}$ and $\tilde{v}^t_{0,1} < v^t_{0,1}$ on the basis of Eq. (33), and this is borne out in Figs. 20 and 21.

Equation (33) suggests that $v^p_{T,S}, \tilde{v}^p_{T,S}$, will be the same for $p=q$, b, and bb. That these quantities differ, however, may be expected for several reasons. The correct $\bar{E}$ for Eq. (33) should depend somewhat on $\vec{L}$ for the intermediate states. The NN states can be coupled to NΔ and ΔΔ states with both higher and lower $\vec{L}$ values, with different centrifugal barriers. Also our choice of no $\vec{L}$ dependence for the $N\Delta(O_{ij}^{p=21-23})$ and $\Delta\Delta(O_{ij}^{p=26-28})$ potentials will have some effect. Unfortunately we have no simple arguments that predict the way these quantities differ.

The remaining elements of the v_{28} model are shown in Fig. 22. The dotted lines show $Y_\pi(r)$ of Eq. (3) and $T_\pi(r)$ of Eq. (4). All twelve transition operator components of v_{28} are proportional to either $Y_\pi(r)$ or $T_\pi(r)$, as given by Eqs. (20)–(22). The solid line shows the projected $\tilde{v}^c(r)$, which is identical to the central interactions $\tilde{v}^{cV}(r)$ in NΔ and $\tilde{v}^{cVII}(r)$ in ΔΔ channels, as per Eqs. (23) and (24). For comparison, $v^c(r)$ is also shown by a dashed line. As suggested by Eq. (33), the differences between $v^p(r)$ and $\tilde{v}^p(r)$ for $p=2$–14 tend to be much smaller, and we do not show them.

The difference between the v_{14} and v_{28} models in $T=0$ states is due to coupling to ΔΔ intermediate states only, but in $T=1$ states the difference is due to both NΔ and

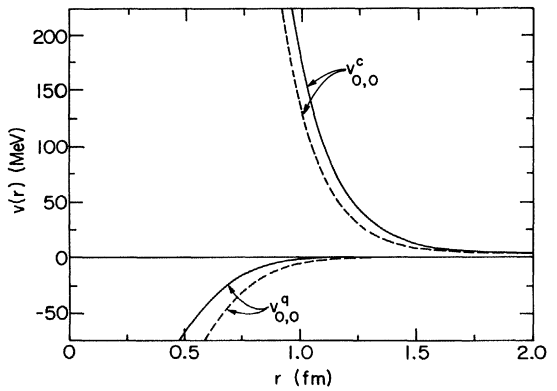

FIG. 17. $T=0,S=0$ central and $\vec{L}^2$ potentials: solid and dashed lines show v_{28} and v_{14} models.

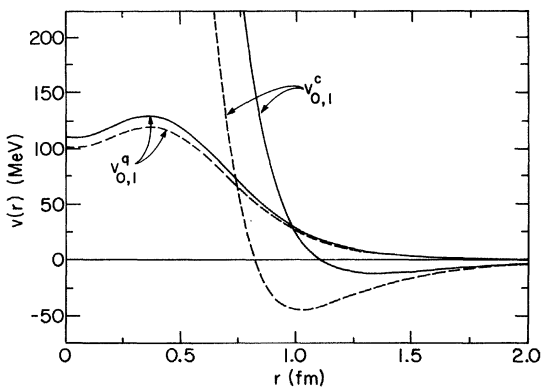

FIG. 19. $T=0,S=1$ central and $\vec{L}^2$ potentials: solid and dashed lines show v_{28} and v_{14} models.

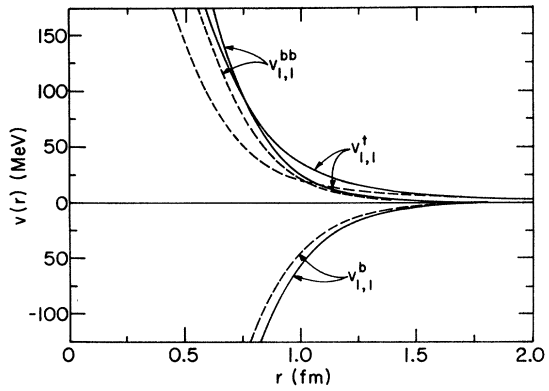

FIG. 20. $T=1,S=1$ tensor, $\vec{L}\cdot\vec{S}$ and $(\vec{L}\cdot\vec{S})^2$ potentials: solid and dashed lines show v_{28} and v_{14} models.

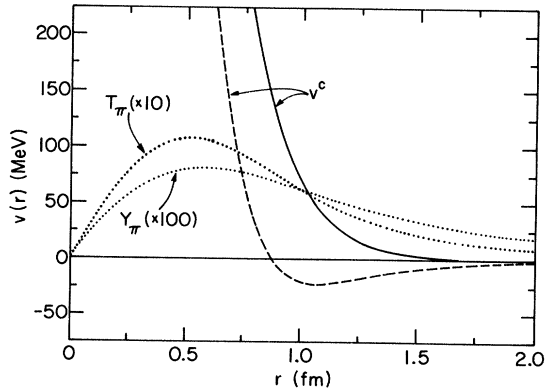

FIG. 22. Transition potential shapes $Y_\pi(r), T_\pi(r)$ are shown with the dotted lines, central potentials $v^c(r)$ in the v_{14} model are shown by the dashed line, and in v_{28} by the solid line; the latter also gives central interaction in NΔ and ΔΔ channels.

ΔΔ states. To get some feeling for the relative importance of the NΔ and ΔΔ contributions, we also fitted the $T=1,S=0$ parameters with the restriction of coupling only to NΔ states. This is equivalent to a v_{21} model with $O_{ij}^{p=1-16,19-23}$. Assuming the same transition and NΔ interactions as in the v_{28} model, we obtained a phase equivalent data fit with (in MeV) $I^c_{1,0}=-3.726$, $I^q_{1,0}=0.05$, $S^c_{1,0}=1826$, and $S^q_{1,0}=132$. The resulting $v^c_{1,0}(r)$, $v^q_{1,0}(r)$ are shown in Fig. 16 by dotted lines. The curves suggest that most of the difference between v_{14} and v_{28} models in $T=1$ states comes from the NΔ intermediate states. The closure argument of Eq. (33) agrees with this.

The choice of the specific forms of the potential models involves a number of arbitrary decisions. The need for (approximately) 14 operators in the NN channel to obtain satisfactory data fits seems to be empirically established by recent models such as Urbana,[6] parametrized Paris,[8] and the present work. Taking the long-range OPE part as given, one then needs at least two functional shapes, of intermediate and short range, to construct reasonable potentials (assuming one is not following a dispersion-theoretic approach). The choice of these shapes, and the manner in which the OPE contribution is cutoff at short distances is arbitrary. (Data fitting does seem easier, however, when the long- and intermediate-range functions vanish at $r=0$,

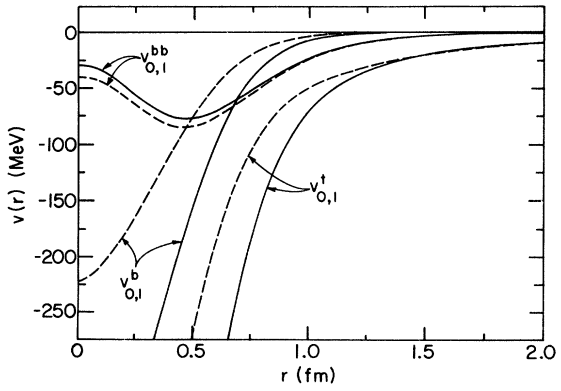

FIG. 21. $T=0,S=1$ tensor, $\vec{L}\cdot\vec{S}$ and $(\vec{L}\cdot\vec{S})^2$ potentials: solid and dashed lines show v_{28} and v_{14} models.

as is the case in our models.) In this sense, the v_{14} model is a "minimal" potential with as few parameters as the data requires.

The addition of Δ(1232) degrees of freedom could produce many more operator components than the 14 we have added to obtain our v_{28} model, and thus introduce many additional parameters. We have included all possible πNΔ and πΔΔ couplings, plus a central repulsion in NΔ and ΔΔ channels. There could be other spin, isospin, tensor, and spin-orbit components in the NΔ and ΔΔ channels, and there could also be intermediate-range contributions to the transition potentials, e.g., from cross-box diagrams, as illustrated in Figs. 6(c) and (d), which we have not allowed. Our restrictions were made to keep the set of parameters to be fit the same as in the v_{14} model, and in this sense the v_{28} is a minimal model also.

Other strategies might be followed in constructing NN potentials with Δ(1232) degrees of freedom. Since the iterated OPE contributions with intermediate NΔ and ΔΔ states are effectively of intermediate range, we initially hoped to keep the short-range $v^p_S(r)$ the same in the v_{28} model, but it was not possible to obtain good data fits. However, it might be possible to fix the short range part from the v_{14} model and compensate by allowing intermediate-range parts in the transition potentials, or a more general potential in the NΔ and ΔΔ channels. Another approach would explicitly introduce ρ-meson potentials, although in a sense these are already included in the cutoff for $T_\pi(r)$ Eq. (4).

The main problem we face in constructing models such as v_{28} is the insensitivity of low-energy NN data to details of the NΔ and ΔΔ potentials. It may be possible to restrict our choices by fitting data in the inelastic region, $E_{\rm lab}>400$ MeV. Several groups have studied this problem,[55–57] with varying degrees of success. It seems difficult to fit both phase shifts and inelasticities at the same time. Also, most of the studies have been limited to NN and NΔ channels, which should be the most important contributors in $T=1$ states, but the addition of ΔΔ channels would seem desirable for $T=0$ states. It should be possible to extend our type of model if two technical improvements are made: relativity must be incorporated and

the width of the Δ must be taken into account. Since the inelasticities are intimately related to the $\pi N\Delta$ couplings, this data could give us significant constraints on $N\Delta$ potentials.

The chief motive for the present work has been to produce a high-qualtiy, realistic NN potential with $\Delta(1232)$ degrees of freedom that can be readily used in nuclear structure calculations. Many of the processes that appear as many-body forces when only nucleon degrees of freedom are allowed will automatically be included in many-body clusters when such a potential is used. The v_{28} model presented here has an operator structure that is convenient for many-body calculations, and we are currently using it to study the triton and nuclear matter. It will be instructive to compare the results of these studies with the predictions of the phase-equivalent v_{14} model, and the v_{14} model plus phenomenological three-nucleon potentials.[17,36]

ACKNOWLEDGMENTS

We wish to thank Prof. R. A. Arndt, Dr. F. Coester, Dr. B. D. Day, Dr. J. L. Friar, Prof. A. D. Jackson, and Dr. S. C. Pieper for their encouragement, assistance, and comments. This work was supported in part by the U.S. Department of Energy under Contracts W-31-109-ENG-38 and DE-AC02-76ER13001 and the National Science Foundation under Grant PHY-8206325.

*Present address: Department of Physics, University of Arizona, Tucson, AZ 85721.

[1]C. DeTar, Phys. Rev. D 17, 302 (1978); 17, 323 (1978).
[2]C. S. Warke and R. Shanker, Phys. Rev. C 21, 2643 (1980).
[3]M. Harvey, Nucl. Phys. A352, 326 (1981).
[4]R. V. Reid, Ann. Phys. (N.Y.) 50, 411 (1968).
[5]K. Holinde and R. Machleidt, Nucl. Phys. A247, 495 (1975).
[6]I. E. Lagaris and V. R. Pandharipande, Nucl. Phys. A359, 331 (1981).
[7]A. D. Jackson, D. O. Riska, and B. VerWest, Nucl. Phys. A249, 397 (1975).
[8]W. N. Cottingham, M. Lacombe, B. Loiseau, J. M. Richard, and R. Vinh Mau, Phys. Rev. D 8, 800 (1973); M. Lacombe, B. Loiseau, J. M. Richard, R. Vinh Mau, J. Côté, P. Pirés, and R. de Tourreil, Phys. Rev. C 21, 861 (1980); in this paper we use the name "parametrized Paris" to denote the p^2-dependent potential of the latter paper.
[9]H. A. Bethe, Annu. Rev. Nucl. Sci. 21, 93 (1971).
[10]H. Kümmel, K. H. Lührmann, and J. G. Zabolitzky, Phys. Rep. 36C, 1 (1978).
[11]J. Chauvin, C. Gignoux, J. J. Benayoun, and A. Laverne, Phys. Lett. 78B, 5 (1978).
[12]G. L. Payne, J. L. Friar, B. F. Gibson, and I. R. Afnan, Phys. Rev. C 22, 823 (1980).
[13]J. Carlson and V. R. Pandharipande, Nucl. Phys. A371, 301 (1981).
[14]B. D. Day, Phys. Rev. Lett. 47, 226 (1981).
[15]I. E. Lagaris and V. R. Pandharipande, Nucl. Phys. A359, 349 (1981).
[16]J. Fujita and H. Miyazawa, Prog. Theor. Phys. 17, 360 (1957).
[17]J. Carlson, V. R. Pandharipande, and R. B. Wiringa, Nucl. Phys. A401, 59 (1983).
[18]H. Sugawara and F. von Hippel, Phys. Rev. 172, 1764 (1968).
[19]R. A. Smith and V. R. Pandharipande, Nucl. Phys. A256, 327 (1976).
[20]J. W. Durso, M. Saarela, G. E. Brown, and A. D. Jackson, Nucl. Phys. A278, 445 (1977).
[21]X. Bagnoud, K. Holinde, and R. Machleidt, Phys. Rev. C 24, 1143 (1981).
[22]S. A. Coon, M. D. Scadron, P. C. McNamee, B. R. Barrett, D. W. E. Blatt, and B. H. J. McKellar, Nucl. Phys. A317, 242 (1979).
[23]G. E. Brown and W. Weise, Phys. Rep. 22C, 279 (1975).
[24]A. M. Green, Rep. Prog. Phys. 39, 1109 (1976).
[25]H. J. Weber and H. Arenhövel, Phys. Rep. 36C, 277 (1978).
[26]A. M. Green and P. Haapakoski, Nucl. Phys. A221, 429 (1974).
[27]A. M. Green and J. A. Niskanen, Nucl. Phys. A249, 493 (1975).
[28]B. D. Day and F. Coester, Phys. Rev. C 13, 1720 (1976).
[29]K. Holinde and R. Machleidt, Nucl. Phys. A280, 429 (1977).
[30]B. D. Day, Rev. Mod. Phys. 50, 495 (1978).
[31]V. R. Pandharipande and R. B. Wiringa, Rev. Mod. Phys. 51, 821 (1979).
[32]G.-H. Niephaus, M. Gari, and B. Sommer, Phys. Rev. C 20, 1096 (1979).
[33]H. Arenhövel, Z. Phys. A 275, 189 (1975).
[34]R. B. Wiringa (unpublished).
[35]W. Manzke and M. Gari, Nucl. Phys. A312, 457 (1978).
[36]R. B. Wiringa, Nucl. Phys. A401, 86 (1983); the parameters given in this reference for Argonne v_{14} were inadvertently rounded and should be replaced by those of Table I in the present work.
[37]R. A. Arndt and L. D. Roper, Scattering Analyses Interactive Dial-in (SAID) program of the Center for Analysis of Particle Scattering, Department of Physics, Virginia Polytechnic Institute and State University.
[38]A. R. Edmonds, *Angular Momentum in Quantum Mechanics* (Princeton University Press, Princeton, NJ, 1957).
[39]J. A. Niskanen, Phys. Lett. 107B, 344 (1981).
[40]M. Gari, H. Hyuga, and B. Sommer, Phys. Rev. C 14, 2196 (1976); note there should be a factor of $\frac{1}{6}$ multiplying $F_M^2(q^2)$ in Eq. (22).
[41]A. H. Wapstra and K. Bos, At. Data Nucl. Data Tables 20, 1 (1977).
[42]R. V. Reid and M. L. Vaida, Phys. Rev. Lett. 29, 494 (1972); 34, 1064(E) (1975).
[43]K. Stephenson and W. Haeberli, Phys. Rev. Lett. 45, 520 (1980).
[44]H. P. Noyes, Annu. Rev. Nucl. Sci. 22, 465 (1972).
[45]J. J. Moré, B. S. Garbow, and K. E. Hillstrom, Argonne National Laboratory Report ANL-80-74, 1980.
[46]S. Galster, H. Klein, J. Moritz, K. H. Schmidt, D. Wegener, and J. Bleckwenn, Nucl. Phys. B32, 221 (1971).
[47]E. L. Lomon, Ann. Phys. (N.Y.) 125, 309 (1980).
[48]E. Hadjimichael, Nucl. Phys. A312, 341 (1978).
[49]G. Höhler, E. Pietarinen, I. Sabba-Stefanescu, F. Borkowski, G. G. Simon, V. H. Walther, and R. D. Wendling, Nucl. Phys. B114, 505 (1976).

[50]G. Lindstrom, Phys. Rev. 78, 817 (1950); Particle Data Group, Rev. Mod. Phys. 52, S1 (1980).
[51]F. Coester and A. Ostebee, Phys. Rev. C 5, 1836 (1975).
[52]H. Arenhövel and W. Fabian, Nucl. Phys. A282, 397 (1977).
[53]A. Cambi, B. Mosconi, and P. Ricci, Phys. Rev. Lett. 48, 462 (1982).
[54]W.-Y. P. Hwang, J. T. Londergan, and G. E. Walker, Ann. Phys. (N.Y.) 149, 335 (1983).
[55]W. M. Kloet and R. R. Silbar, Nucl. Phys. A338, 281 (1980); A338, 317 (1980).
[56]M. Betz and T.-S. H. Lee, Phys. Rev. C 23, 375 (1981).
[57]B. Blankleider and I. R. Afnan, Phys. Rev. C 24, 1572 (1981).